Physics Letters B 700 (2011) 207–216

Contents lists available at ScienceDirect

Physics Letters B

www.elsevier.com/locate/physletb

Non-Abelian discrete dark matter

Adisorn Adulpravitchai [a], Brian Batell [b,*], Josef Pradler [b]

[a] Max-Planck-Institut für Kernphysik, Postfach 10 39 80, 69029 Heidelberg, Germany
[b] Perimeter Institute for Theoretical Physics, Waterloo, ON, N2L 2Y5, Canada

ARTICLE INFO

Article history:
Received 29 March 2011
Accepted 6 April 2011
Available online 20 April 2011
Editor: A. Ringwald

Keywords:
Dark matter

ABSTRACT

We consider the minimal model in which dark matter is stabilized by a non-Abelian discrete symmetry. The symmetry group is taken to be $D_3 \cong S_3$, which is the smallest non-Abelian finite group. The minimal model contains (nontrivial) singlet and doublet scalar representations of D_3 which couple to the Standard Model fields via the Higgs portal. This construction predicts two species of dark matter over much of the parameter space. Nontrivial interactions under D_3 lead to a novel thermal history of dark matter, while the multi-component nature of dark matter can be tested by future direct detection experiments.

Understanding the nature of the cosmological dark matter (DM) that constitutes one quarter of the energy density of the universe is a central goal of particle physics today [1]. While there is little room left to doubt the existence of DM, its microscopic properties are virtually unknown. One of the few properties in which we can be confident is that DM should be stable on time scales greater than the age of the universe, suggesting the existence of a new "dark" symmetry. But precisely what symmetry stabilizes DM is a mystery.

Many models employ a discrete Z_2 symmetry to stabilize DM. This Z_2 symmetry is often motivated by the need to suppress dangerous operators in new physics scenarios that solve the hierarchy problem. However, given that we have no experimental indication of what new physics, if any, addresses the naturalness issues in the SM, one may take a more general perspective regarding DM and the symmetries responsible for its stability. More pragmatically, the exploration of alternative stabilizing symmetries is warranted by the prospect of novel phenomena associated with DM, as such symmetries may predict new states and interactions.

Indeed, there are many possibilities other than a Z_2-parity that can protect DM against decay. In particular, besides the Abelian cyclic symmetry Z_N [2], DM may well be stabilized by a non-Abelian discrete symmetry. Non-Abelian finite groups have received some limited attention within the context of DM. Motivated by improved gauge coupling unification, Ref. [3] considered an additional Higgs doublet in a non-Abelian discrete multiplet serving as DM. Non-Abelian discrete symmetries also lead to distinct decay patterns in decaying dark matter scenarios [4,5]. *Continuous* non-Abelian symmetries originating from broken or confined gauge theories can also ensure DM stability [6]. Models of DM stabilized by *Abelian* discrete symmetries that descend from higher non-Abelian ones have been motivated by astrophysical anomalies [7], discrete gauge symmetries [8], and neutrino physics [9]. Indeed, non-Abelian flavor symmetries are widely used to explain the neutrino oscillation data [10] (for recent reviews see Refs. [11,12]). Such non-Abelian discrete symmetries can come from the breaking of continuous flavor symmetries [13] or from orbifold compactification of extra-dimensions [14].

In this Letter we construct the minimal model of DM in which stability is a consequence of a non-Abelian discrete symmetry. The model follows in spirit the canonical scalar Standard Model (SM) singlet models of Refs. [15–17]. The symmetry group we consider is D_3, the dihedral group of order 6, which is the smallest non-Abelian finite group. It is isomorphic to S_3, the permutation symmetry of three objects. We determine the minimal field content of the model and couple it to the SM via renormalizable Higgs portal interactions. Over much of the parameter space, the D_3 symmetry predicts two species of DM, which can contribute to the cosmological abundance. We investigate in detail the cosmology of the model, finding that nontrivial interactions under D_3 in the dark sector lead to a novel thermal history. We also analyze the constraints and prospects at direct detection experiments. In particular we find that the two-component nature of DM can be discovered in future ton-scale experiments.

1. D_3 stabilization of dark matter

We start by constructing the minimal model of DM stabilized by a non-Abelian discrete symmetry. The model is based on the

* Corresponding author.
E-mail addresses: a.adulpravitchai@mpi-hd.mpg.de (A. Adulpravitchai), bbatell@perimeterinstitute.ca (B. Batell), jpradler@perimeterinstitute.ca (J. Pradler).

0370-2693
doi:10.1016/j.physletb.2011.04.015

group D_3, which is the smallest non-Abelian discrete symmetry group and describes the symmetry properties of the equilateral triangle. The group contains two generators, A and B, obeying the properties

$$A^3 = 1, \qquad B^2 = 1, \qquad ABA = B, \tag{1}$$

and the six group elements are constructed through combinations of the two generators: 1, A, A^2, B, BA, BA^2. The group D_3 has two singlet and one doublet representation, denoted, $\underline{\mathbf{1}}_{\mathbf{1}}$, $\underline{\mathbf{1}}_{\mathbf{2}}$, and $\underline{\mathbf{2}}$ respectively. The singlet $\underline{\mathbf{1}}_{\mathbf{1}}$ transforms trivially under D_3, $A = B = 1$, while the generators of the (nontrivial) singlet representation $\underline{\mathbf{1}}_{\mathbf{2}}$ are $A = 1$ and $B = -1$. The generators for the doublet representation $\underline{\mathbf{2}}$ are

$$A = \begin{pmatrix} e^{2\pi i/3} & 0 \\ 0 & e^{-2\pi i/3} \end{pmatrix}, \qquad B = \begin{pmatrix} 0 & 1 \\ 1 & 0 \end{pmatrix}. \tag{2}$$

The multiplication rules for the singlet representations are given by

$$\underline{\mathbf{1}}_{\mathbf{1}} \otimes \underline{\mathbf{1}}_{\mathbf{1}} = \underline{\mathbf{1}}_{\mathbf{1}}, \qquad \underline{\mathbf{1}}_{\mathbf{2}} \otimes \underline{\mathbf{1}}_{\mathbf{2}} = \underline{\mathbf{1}}_{\mathbf{1}}, \quad \text{and} \quad \underline{\mathbf{1}}_{\mathbf{1}} \otimes \underline{\mathbf{1}}_{\mathbf{2}} = \underline{\mathbf{1}}_{\mathbf{2}}, \tag{3}$$

whereas the product of two doublets, $\underline{\mathbf{2}} \otimes \underline{\mathbf{2}}$ decomposes into two singlets and one doublet as

$$(a_1 b_2 + a_2 b_2) \sim \underline{\mathbf{1}}_{\mathbf{1}}, \qquad (a_1 b_2 - a_2 b_2) \sim \underline{\mathbf{1}}_{\mathbf{2}}, \qquad \begin{pmatrix} a_2 b_2 \\ a_1 b_1 \end{pmatrix} \sim \underline{\mathbf{2}}, \tag{4}$$

where $(a_1, a_2)^T, (b_1, b_2)^T \sim \underline{\mathbf{2}}$; for further formulae of dihedral groups, see, *e.g.*, [18,19,12].

The minimal model of DM having nontrivial properties under D_3 contains two scalar fields,

$$\eta, \qquad X \equiv \begin{pmatrix} \chi \\ \chi^* \end{pmatrix}, \tag{5}$$

which transform as a singlet $\underline{\mathbf{1}}_{\mathbf{2}}$ and doublet $\underline{\mathbf{2}}$, respectively. The scalar η is real while χ is complex, which amounts to a total of three new degrees of freedom. Along with the SM Higgs field H, the scalar sector of the Lagrangian contains kinetic terms and a potential. The general renormalizable scalar potential invariant under D_3 and the SM gauge symmetries may be constructed using Eqs. (3), (4) and reads

$$\begin{aligned} V = {} & m_1^2 H^\dagger H + \frac{1}{2} m_2^2 \eta^2 + m_3^2 \chi^* \chi + \frac{\mu_1}{3!}(\chi^3 + \chi^{*3}) \\ & + \lambda_1 (H^\dagger H)^2 + \frac{\lambda_2}{4} \eta^4 + \lambda_3 (\chi^* \chi)^2 \\ & + \alpha_1 (H^\dagger H) \eta^2 + 2\alpha_2 (H^\dagger H)(\chi^* \chi) + \alpha_3 \eta^2 (\chi^* \chi) \\ & + \frac{i\alpha_4}{3!} \eta (\chi^3 - \chi^{*3}), \end{aligned} \tag{6}$$

where all parameters in the Lagrangian are real. We note that the theory is invariant under P and C—a fact that will simplify our considerations regarding the relic abundance.

A model with only one scalar field η (χ) can provide a viable theory of DM, but such a theory is equivalent to a theory based on an Abelian discrete Z_2 (Z_3) symmetry. The minimal theory based on the group D_3 contains both scalars, η and χ, and the nontrivial interaction predicted by this symmetry is the last term in the potential (6), with coupling α_4.

We will be interested in the case in which the electroweak symmetry is spontaneously broken while the D_3 discrete symmetry is unbroken,

$$\langle H \rangle = \frac{1}{\sqrt{2}} \begin{pmatrix} 0 \\ v \end{pmatrix}, \qquad \langle \eta \rangle = 0, \qquad \langle \chi \rangle = 0, \tag{7}$$

where $v^2 \equiv -m_1^2/\lambda_1 \simeq (246\ \text{GeV})^2$ is the (squared) Higgs vacuum expectation value. We demand that the potential is bounded from below, and that the electroweak vacuum is the global minimum of the potential. These requirements constrain the values of the coupling constants in the potential. Qualitatively, the quartic couplings $\lambda_{1,2,3}$ must be positive, $\alpha_{1,2,3}$ must be greater than some minimum (negative) value, and the magnitude of α_4 must be smaller than some maximum value. Furthermore, the mass parameters $m_{2,3}^2$ should not be too large and the magnitude of the cubic coupling μ_1 is bounded from above. Throughout our analysis, we have verified numerically that our parameter choices lead to a stable potential and electroweak vacuum. One may also investigate the vacuum structure of the theory at higher energy scales using a renormalization group analysis (as, *e.g.*, in Ref. [20]), but here we will be content to consider Eq. (6) a low energy effective theory of DM defined around the weak scale.

Expanding around the vacuum (7) with $v \to v + h$, we derive the following potential:

$$\begin{aligned} V = {} & \frac{1}{2} m_h^2 h^2 + \frac{1}{2} m_\eta^2 \eta^2 + m_\chi^2 \chi^* \chi \\ & + \lambda_1 v h^3 + \alpha_1 v h \eta^2 + 2\alpha_2 v h (\chi^* \chi) + \frac{\mu_1}{3!}(\chi^3 + \chi^{*3}) \\ & + \frac{\lambda_1}{4} h^4 + \frac{\lambda_2}{4} \eta^4 + \lambda_3 (\chi^* \chi)^2 \\ & + \frac{\alpha_1}{2} h^2 \eta^2 + \alpha_2 h^2 (\chi^* \chi) + \alpha_3 \eta^2 (\chi^* \chi) \\ & + \frac{i\alpha_4}{3!} \eta (\chi^3 - \chi^{*3}), \end{aligned} \tag{8}$$

where the physical masses are

$$\begin{aligned} m_h^2 &\equiv 2\lambda_1 v^2, \\ m_\eta^2 &\equiv m_2^2 + \alpha_1 v^2, \\ m_\chi^2 &\equiv m_3^2 + \alpha_2 v^2. \end{aligned} \tag{9}$$

The nontrivial interaction predicted by the D_3 symmetry, with coupling α_4, allows the scalar η to decay via $\eta \to 3\chi, 3\chi^*$ if $m_\eta > 3m_\chi$. In this case, χ is the only stable DM candidate. If, however, $m_\eta < 3m_\chi$ these decays are kinematically forbidden, and both η and χ are stable. Therefore, the D_3 model predicts two species of DM for $m_\eta < 3m_\chi$.

2. Cosmology

We now examine the thermal history of the η and χ particles in the minimal D_3 model. The cosmic relic abundances of these particles are governed by Boltzmann equations that account for the expansion of the universe as well as for reactions that change the total number of particles for the species of interest. If these reactions freeze out when the temperature is not too much smaller than the mass of the particle, there will be associated a significant energy density that remains today that may account for the observed DM in the universe.

From the potential in Eq. (8), we can determine the reactions that change the total number of particles, which may be classified as follows:

(a) *Annihilation into SM*:

$$\eta\eta \to t\bar{t}, hh, ZZ, WW, b\bar{b} \ldots,$$
$$\chi\chi^* \to t\bar{t}, hh, ZZ, WW, b\bar{b} \ldots.$$

(b) *Semi-annihilation*:

$$\chi\chi \to h\chi^*, \qquad \chi h \to \chi^*\chi^*.$$

(c) *DM conversion*:

$$\eta\chi \to \chi^*\chi^*, \qquad \eta\chi^* \to \chi\chi, \qquad \chi\chi \to \eta\chi^*,$$
$$\eta\eta \to \chi\chi^*, \qquad \chi\chi^* \to \eta\eta.$$

(d) *Late decay*:

$$\eta \to 3\chi, 3\chi^*.$$

The reactions listed above constitute the relevant processes that change the number of η and χ particles; analogous reactions hold for χ^*. (Annihilation into three body final states can be important right below the WW threshold [21].) We see that the D_3 symmetry allows for the non-canonical processes of semi-annihilation (b) and DM conversion (c), studied recently in Refs. [6,22], as well as a late decay scenario (d) [23]. *CP* invariance of the potential (6) implies $n_{\chi^*} = n_\chi$ so that we only need to solve the Boltzmann equation for n_χ; the total relic density is then $n_{\chi+\chi^*} = 2n_\chi$. Furthermore, processes (b), (c), and (d) couple the Boltzmann equations for η and χ.

We have performed a general analysis of the Boltzmann equations following the usual treatments of Refs. [24–27], with modifications for semi-annihilation and DM conversion; a summary is presented in Appendix A. In the results presented below, we obtain the relic densities of η and χ by numerically integrating the coupled set of equations. We now present a detailed survey of the cosmology, emphasizing the novel aspects that are a result of the D_3 symmetry.

An immediate consequence of the non-Abelian symmetry is that since there are two stable DM candidates for $m_\eta < 3m_\chi$, the individual relic abundances are not fixed by the WMAP measurement of the DM relic density, but rather the sum is fixed: $\Omega_\eta h^2 + \Omega_{\chi+\chi^*}h^2 = \Omega_{DM}^{\rm WMAP}h^2 = 0.1126 \pm 0.0036$ [28]. This means that different choices for a certain combination of parameters will fit the WMAP measurement while shifting the fractional abundances of η and χ.

2.1. Annihilation into SM

The first class of reactions (a) in which η and χ annihilate into light SM particles is common to any scalar DM model with a Higgs portal interaction. In the case $m_{\chi,\eta} \ll m_h$, the thermally averaged annihilation cross section may be written as [15–17]

$$\langle\sigma v\rangle_{ii\to X_{SM}} \simeq \frac{4\alpha_i^2 v^2}{(4m_i^2 - m_h^2)^2 + m_h^2\Gamma_h^2}\frac{\widetilde{\Gamma}_i}{m_i}, \tag{10}$$

where $i = 1$ (2) corresponds to η (χ) and X_{SM} denotes all kinematically allowed final states (*e.g.*, $X_{SM} = ZZ, WW, b\bar{b}, \ldots$ for $m_i > m_Z$); v in the nominator of the right-hand side stands of course for the Higgs expectation value in (7). Furthermore, Γ_h denotes the decay width of the SM Higgs boson (including decays to the new dark scalars if kinematically accessible) and we have defined $\widetilde{\Gamma}_i \equiv \Gamma_{h^*\to X_{SM}}(m_{h^*} = 2m_i)$ to denote the decay width of a virtual SM Higgs of mass $m_{h^*} = 2m_i$. For scalars above the weak scale, $m_{\eta,\chi} \gg m_h$, the annihilation cross section becomes

$$\langle\sigma v\rangle_{ii\to X_{SM}} \simeq \frac{\alpha_i^2}{4\pi m_i^2}. \tag{11}$$

For the lightest of the DM species, annihilation into SM final states is particularly important since the DM conversion processes (c) are likely suppressed by kinematics and Boltzmann statistics. Consider, for concreteness, the case $m_\eta < m_\chi$ for which η dominantly depletes via annihilation into the SM final states. This implies a sizable Higgs portal coupling α_1 in order to obtain an acceptable relic density. For example, for $m_\eta \ll m_h$ and below the s-channel resonance at $m_\eta = m_h/2$, the dominant annihilation channel is $\eta\eta \to b\bar{b}$, with cross section $\langle\sigma v\rangle_{\eta\eta\to b\bar{b}} \simeq 3\alpha_1^2 m_b^2/\pi m_h^4$. One then finds a minimal coupling $\alpha_1 \gtrsim 0.2 \times (m_h/120\ \text{GeV})^2$. Also in the opposite case, when η is heavier than the SM Higgs h (but still lighter than χ), the annihilation cross section (11) dictates a minimal coupling $\alpha_1 \gtrsim 0.1 \times (m_\eta/600\ \text{GeV})$. Only near resonance, $m_\eta = m_h/2$, can the coupling α_1 be much smaller while still allowing for sufficient depletion of η particles. Conversely, the heavier species χ need not couple strongly to the Higgs portal since the DM conversion processes (c) are efficient for $m_\chi > m_\eta$.

2.2. Semi-annihilation

Consider now the case when χ is lighter than η. The Higgs portal coupling α_2 should now be sizable to give χ the right relic abundance. In addition, the semi-annihilation processes (c) become available for $m_\chi > m_h$. Indeed, this may be the dominant process for which one can obtain a semi-analytic solution to the relic abundance of χ [22]:

$$\Omega_{\chi+\chi^*}h^2 \simeq 2 \times \frac{1.07 \times 10^9 x_F}{g_*^{1/2} M_P [\frac{1}{2}\langle\sigma v\rangle_{\chi\chi\to\chi^* h}]}; \tag{12}$$

g_* denotes the effective number of relativistic degrees of freedom at the time of the freeze-out, and the Planck scale is $M_P = 1.22 \times 10^{19}$ GeV. The decoupling temperature T_F can be determined upon solution of $x_F \simeq \log\{0.038c(c+1)[\frac{1}{2}\langle\sigma v\rangle_{\chi\chi\to\chi^* h}] \times m_\chi M_P g_*^{-1/2} x_F^{-1/2}\}$ with $c = \sqrt{2} - 1$, where $x = m_\chi/T$. In the D_3 model the thermally averaged semi-annihilation cross section is given by

$$\langle\sigma v\rangle_{\chi\chi\to h\chi^*} \simeq \frac{3\alpha_2^2\mu_1^2 v^2}{32\pi m_\chi^6}. \tag{13}$$

We see from Eq. (13) that both the Higgs portal coupling α_2 and the cubic coupling μ_1 must be nonzero for semi-annihilation to play a role. Because $\alpha_2 \neq 0$, annihilation into SM final states (a) can occur as well and will in general dominate unless the coupling μ_1 is relatively large. Furthermore, because of the steep falloff of the semi-annihilation cross section (13) with increasing m_χ, the process is most effective when χ is not much heavier than the SM Higgs, $m_\chi \gtrsim m_h$. The effect of semi-annihilation is illustrated in Fig. 1, which shows the evolution of the comoving density $Y \equiv n/s$, where s is the entropy density.

2.3. DM conversion

We next consider the processes of DM conversion (d), which consist of $2 \to 2$ reactions that convert DM of one species into another. There are two types of reactions within class (d) that may be distinguished. The reactions in the first line of (d) may be regarded as "dark" semi-annihilation (*e.g.*, $\chi\chi \to \eta\chi^*$, etc.), in which the number of DM particles of a particular species changes by one unit. Such processes are governed by the nontrivial interaction predicted by the D_3 symmetry in Eq. (6) with coupling α_4. The reactions in the second line of (d) are regarded as "dark" annihilation (*e.g.*, $\chi\chi^* \to \eta\eta$ and the inverse process), which change the number of each dark species by two units. The dark annihilation processes can be mediated by the Higgs portal when $\alpha_{1,2}$ are sizable, or via the direct scalar coupling α_3 in Eq. (6).

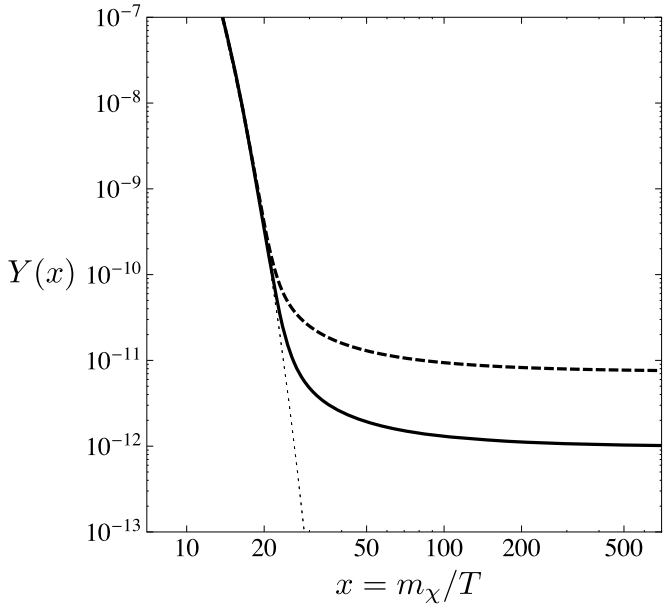

Fig. 1. *Semi-annihilation*: The comoving density $Y(x)$ vs. $x = m_\chi/T$ for χ. The thin dotted line shows the equilibrium value $Y^{\rm eq}(x)$, while the thick lines show the evolution of the comoving density. We take $m_\chi = 200$ GeV, $m_h = 120$ GeV, $\alpha_2 = 0.016$, and $\alpha_1 = \alpha_3 = \alpha_4 = 0$ while assuming $m_\eta \gg m_\chi$. With $\mu_1 = 0$ (dashed) χ freezes out too early and overcloses the universe whereas with $\mu_1 = 1000$ GeV (solid) χ freezes out later so that the relic abundance is $\Omega_{\chi+\chi^*} = \Omega_{DM}^{\rm WMAP}$ despite such a small value of the Higgs portal coupling α_2. This illustrates that semi-annihilation allows for efficient depletion of χ if the cubic coupling μ_1 is sizable when $m_\chi > m_h$.

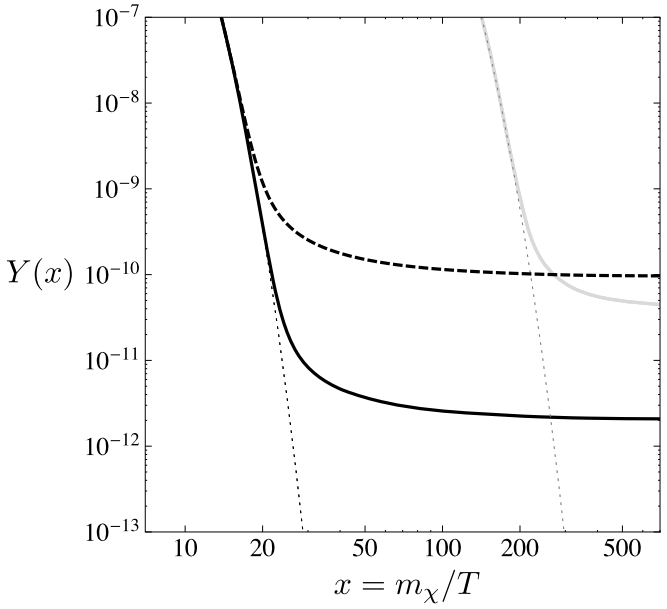

Fig. 2. *DM Conversion*: The comoving density $Y(x)$ vs. $x = m_\chi/T$ for η (gray) and χ (black). The thin dotted lines show the equilibrium value $Y^{\rm eq}(x)$, while the thick lines show the evolution of the comoving density. We take $m_\eta = 5$ GeV, $m_\chi = 50$ GeV, $m_h = 120$ GeV, $\alpha_1 = 0.45$, and $\mu_1 = \alpha_2 = \alpha_3 = 0$. With $\alpha_4 = 0.01$ (dashed black) χ freezes out too early and overcloses the universe whereas with $\alpha_4 = 0.075$ (solid black) χ freezes out later so that the total relic abundance is $\Omega_\eta + \Omega_{\chi+\chi^*} = \Omega_{DM}^{\rm WMAP}$. This demonstrates that DM conversion is very efficient at depleting the heavier DM species χ. Conversely, the relic abundance of the lighter species η is the same for both values of α_4 and therefore not affected by DM conversion.

The DM conversion processes that reduce the number of the heavier DM species, be it η or χ, are kinematically favorable and hence very efficient at depleting such heavy particles. Thus DM conversion may have a dramatic influence on the eventual number density of the heavier species. Unless the masses of DM particles are nearly degenerate, the relic abundance of the lighter DM species will not be influenced.

Let us illustrate the effect of DM conversion by assuming for the moment that $m_\chi \gg m_\eta$ for which there are two stable DM species. As discussed above, η—being the lighter state—must have a sizable Higgs portal coupling α_1. On the other hand, χ may deplete via DM conversion processes. For example, if the dominant process is $\chi\chi \to \eta\chi^*$, the relic abundance may be estimated from (12) with the replacement $\langle\sigma v\rangle_{\chi\chi\to\chi^* h} \to \langle\sigma v\rangle_{\chi\chi\to\eta\chi^*}$. In our minimal D_3 model the "dark" semi-annihilation cross section is found to be

$$\langle\sigma v\rangle_{\chi\chi\to\eta\chi^*} \simeq \frac{3\alpha_4^2}{128\pi m_\chi^2}. \tag{14}$$

One needs in this case a minimal coupling $\alpha_4 \gtrsim 0.05 \times (m_\chi/50\ \text{GeV})$. In contrast to semi-annihilation into the SM Higgs (13), "dark" semi-annihilation (14) is quite efficient and requires only a modest coupling α_4 to significantly influence the relic abundance of χ. We illustrate the effect of DM conversion in Fig. 2, focusing on "dark" semi-annihilation. A similar discussion applies to "dark" annihilation (*e.g.*, $\chi\chi^* \to \eta\eta$, etc.).

2.4. Late decay of η

The final novel aspect of the cosmology in the minimal D_3 model is the possibility of the late decay of η. If $m_\eta > 3m_\chi$, the state η will decay via $\eta \to 3\chi, 3\chi^*$ due to the coupling α_4. In the limit $m_\eta \gg 3m_\chi$, the total width of η is approximately given by

$$\Gamma_\eta \simeq \frac{\alpha_4^2 m_\eta}{1536\pi^3}, \tag{15}$$

and which implies a lifetime of

$$\tau_\eta \simeq 10^{-8}\ \text{s} \times \left(\frac{10^{-7}}{\alpha_4}\right)^2 \left(\frac{100\ \text{GeV}}{m_\eta}\right). \tag{16}$$

For small values of α_4 (which are technically natural), η becomes long-lived in the sense that it decays after chemical decoupling, $\tau_\eta \gg t_{\eta,F}$. The cosmic time at freeze-out reads $t_{\eta,F} \simeq 10^{-8}\ \text{s} \times (m_\eta/100\ \text{GeV})^{-2}(x_{\eta,F}/20)^2$, where $x_\eta \equiv m_\eta/T$ and $T_{\eta,F}$ is the decoupling temperature. For a given m_η, it is then easy to read off the maximum values of α_4 from (16) so that the late-decay condition $\tau_\eta \gg t_{\eta,F}$ holds. Clearly, the decays $\eta \to 3\chi, 3\chi^*$ can then significantly contribute to the relic abundance $\Omega_{\chi+\chi^*}h^2$—provided that χ-annihilation has frozen out. In the limit where χ is initially depleted, late η-decays lead to a non-thermal χ-population with relic DM abundance

$$\Omega_{\chi+\chi^*}h^2 = 3\frac{m_\chi}{m_\eta}\Omega_\eta h^2, \tag{17}$$

where $\Omega_\eta h^2$ represents the would-be relic abundance of η particles today, had they not decayed. The late decay scenario is illustrated in Fig. 3.

For $\tau_\eta > 1$ s, the late-decay scenario (d) is cosmologically constrained. The main decay mode $\eta \to 3\chi^{(*)}$ is inevitably accompanied by $\eta \to 3\chi^{(*)} + h^*$ where the virtual h^* decays into kinematically accessible final states. This leads to electromagnetic and hadronic energy injection into the primordial plasma. If the decay happens during or after Big Bang nucleosynthesis (BBN) the

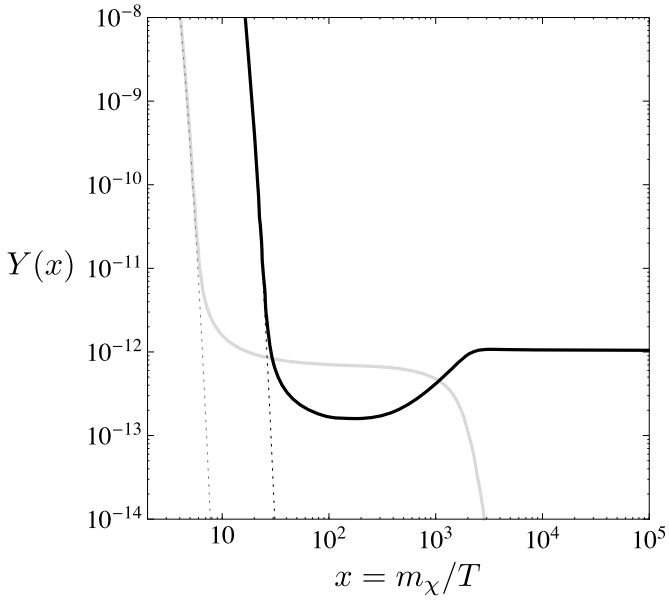

Fig. 3. *Late decay*: The comoving density $Y(x)$ vs. $x = m_\chi/T$ for η (gray) and χ (black). The thin dotted lines show the equilibrium value $Y^{\rm eq}(x)$, while the thick lines show the evolution of the comoving density. We take $m_\eta = 800$ GeV, $m_\chi = 200$ GeV, $m_h = 120$ GeV, $\alpha_1 = 0.11$, $\alpha_2 = 0.15$, $\alpha_4 = 10^{-9}$ and $\mu_1 = \alpha_3 = 0$, leading to a long lifetime $\tau_\eta \sim 40$ μs. Initially χ is depleted through efficient annihilation into SM particles, whereas η freezes out with a significant density. Later, η decays and repopulates χ, χ^* which then comprise the observed DM.

induced spallation reactions of the light elements can spoil the concordance of BBN abundance predictions with their observationally inferred values (for a review see, *e.g.*, [29].) Since energy depositions as small as $\mathcal{O}$(few MeV) per baryon can probed in BBN [30], branching fractions of the $3\chi + h^*$ decay mode of, say, $\mathcal{O}(10^{-4})$ are still constrained. To circumvent this issue as well as potential warm DM constraints due to the free streaming of the decay products χ, one can simply impose $\tau_\eta < 1$ s. For a kinematically unsuppressed decay, this requires $|\alpha_4| \gtrsim 10^{-11}\sqrt{100\ \text{GeV}/m_\eta}$.

Finally, we note that in the limit $\alpha_4 \to 0$, η becomes stable even for $m_\eta > 3m_\chi$. This is easily understood since in this limit the Lagrangian displays a Z_2 symmetry $\eta \to -\eta$ which renders η stable.

3. Direct detection phenomenology

The minimal D_3 model of DM can be efficiently probed by direct detection experiments. Furthermore, compared to the canonical Z_2 scalar singlet model, the non-Abelian D_3 model offers several distinct direct detection signatures which can be observed by current and next generation experiments. We now examine the constraints and future prospects offered by these experiments.

We use the standard formalism [31] to predict the nuclear recoil rates from elastic scattering of η and χ. The differential event rate is given by

$$\frac{dR_i}{dE_R} = N_T \frac{\rho_i}{m_i} \int\limits_{|\boldsymbol{v}| \geqslant v_{\min}} d^3\boldsymbol{v}\, v f(\boldsymbol{v}, \boldsymbol{v}_e) \frac{d\sigma_i}{dE_R}, \tag{18}$$

where $i = 1$ (2) corresponds to η (χ), N_T is the number of target nuclei per unit detector mass, ρ_i is the local DM mass density for a given species, and $f(\boldsymbol{v}, \boldsymbol{v}_e)$ is the DM velocity distribution taken to be Maxwellian and truncated at an escape velocity of $v_{\rm esc} = |\boldsymbol{v} + \boldsymbol{v}_e| = 600$ km/s; $v_{\min}$ is the minimum velocity required to cause a nuclear recoil with energy E_R and $\boldsymbol{v}_e$ and $\boldsymbol{v}$ are the velocity of the earth in the galactic frame and the velocity of the DM particle in the earth's frame, respectively. The theoretical rate in Eq. (18) is corrected to account for potential quenching of the recoil signal as well as for finite detector resolution, efficiency, and acceptance to obtain a prediction for the observed rate. The total number of events in a certain energy interval is then found by integrating the rate and multiplying by the raw exposure.

The microscopic physics of our D_3 model enters into the scattering cross section in Eq. (18). The scalar representation of D_3 gives rise to spin-independent DM-nucleus scatterings. The differential cross section is conventionally expressed as [1],

$$\frac{d\sigma_i}{dE_R} = \frac{m_N}{2v^2} \frac{\sigma_n^{(i)}}{\mu_n^2} \left[\frac{f_p Z + f_n (A - Z)}{f_n}\right]^2 F^2(E_R), \tag{19}$$

where m_N is the mass of the target nucleus, μ_n is the DM-nucleon reduced mass, and $F^2(E_R)$ is the nuclear form factor; we take the Helm form factor following [31] with nuclear skin thickness $s = 0.9$ fm. Spin-independent elastic scattering of the DM particles η and χ with nuclei is mediated via a t-channel exchange of the SM Higgs boson and therefore governed by the couplings α_1 and α_2, respectively. The DM-nucleon cross section is given by

$$\sigma_n^{(i)} = \frac{\alpha_i^2 f_n^2 \mu_n^2}{\pi m_i^2 m_h^4}, \tag{20}$$

where $f_n = \sum_q \langle n|m_q \bar{n} n|n\rangle \simeq 0.52$ GeV is the effective DM-nucleon coupling [32].

Because there are two species of DM in our model, the local density of each species is typically not equal to $\rho_0 \approx 0.3\ \text{GeV}\,\text{cm}^{-3}$. As in Ref. [33] we assume that the local density of each DM particle is proportional to its cosmological abundance, *i.e.*,

$$\rho_i = \frac{\Omega_i}{\Omega_{DM}^{\rm WMAP}} \rho_0. \tag{21}$$

For a given set of model parameters, we compute the relic density Ω_i of each species by integrating the Boltzmann equations, find the local DM mass density ρ_i according to Eq. (21), and calculate the nuclear scattering rate (18).

3.1. Experiments

In the following discussion we shall focus on the liquid xenon experiments in anticipation of the upcoming XENON100 one-year data release as well as the prospect of future ton-scale experiments which have the potential to probe large regions of the D_3 model parameter space. Furthermore, past data sets from XENON10 [34,35] and XENON100 [36] yield current limits on spin-independent scattering that are competitive with other experiments, such as CDMS-II [37,38].

The XENON experiments use a prompt scintillation light signal (S1) and a delayed ionization signal (S2) to discriminate between nuclear and electron recoil events. Recently, there has been a lot of debate on the scintillation yield for nuclear recoils, $\mathcal{L}_{\rm eff}$, as well as on the stochasticity of the S1 signal for lowest E_R. Since $\mathcal{L}_{\rm eff}$ defines the detector threshold, this quantity is of importance when inferring σ_n-limits for small DM masses $\mathcal{O}(10$ GeV) [39,40]. We use the results of the detailed study [40] to account for resolution, efficiency, and acceptance of the XENON10 [34] and XENON100 [36] detectors where we employ the most conservative assumption on $\mathcal{L}_{\rm eff}$ (yielding the weakest limits on σ_n). Constraints are obtained by Yellin's maximum gap method [41] which accounts for the $\mathcal{O}(10)$ events observed in the XENON10 re-analysis [35] of its 316 kg × days data sample. The XENON100 collaboration has published an analysis of an 11 day run yielding a raw exposure of 447 kg × days [36]; no candidate events were observed.

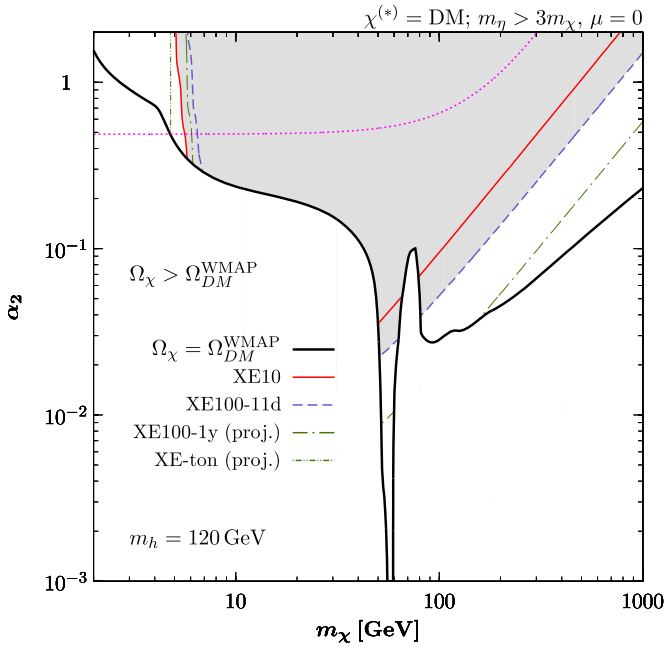

Fig. 4. *Direct detection constraints*: Shown is the m_χ–α_2 plane for $m_\eta > 3m_\chi$ and $\mu = 0$. Along the thick solid (black) line $\Omega_{\chi+\chi^*} = \Omega_{DM}^{\mathrm{WMAP}}$ holds. The region below is excluded, $\Omega_{\chi+\chi^*} > \Omega_{DM}^{\mathrm{WMAP}}$. Only $\chi^{(*)}$ is stable so that above the solid black line $\eta \to 3\chi^{(*)}$ populates $\chi^{(*)}$ such that $\rho_\chi = \rho_0$. The gray shaded region is excluded by current direct detection experiments. As labeled, the lines depict the individual experiments and show their current (projected) sensitivity for exclusion. For $m_\chi \sim m_h/2 = 60$ GeV primordial annihilation can proceed resonantly via Higgs exchange. The horizontal dotted line shows a vacuum stability constraint for $\lambda_3 = 2$; values above are excluded.

In addition, a data release from a one year run of XENON100 is expected shortly. To estimate the reach of this data set we assume an exposure of 100 live days, collected with their fiducial detector mass of 30 kg. Lastly, for the sake of exploring future sensitivity of a ton-scale liquid xenon experiment, following Ref. [42] we assume less than one background event; we take a (moderate) raw exposure of 1 ton × yr. We mimic energy resolution and efficiency of the detector by employing the same analysis [40] as used for the XENON10 detector above; this implies a more optimistic assumption on the low recoil acceptance then had we used the similar analysis for XENON100.

As we now show, large portions of the parameter space in the D_3 model have been or will be probed by liquid xenon experiments. We will describe the constraints and future sensitivities in detail for two novel scenarios that may occur in the D_3 model: 1) the late-decay scenario ($m_\eta > 3m_\chi$), and 2) the two-component DM scenario ($m_\eta < 3m_\chi$).

3.2. Constraints for $m_\eta > 3m_\chi$

If η is more than three times as heavy as χ, it is unstable, dictating that χ accounts for all of the cosmological DM. Without making assumptions about the lifetime of η (or equivalently the coupling α_4), the Higgs portal coupling α_2 can take a range of values and still be consistent with the relic abundance constraint. The minimum allowed value of α_2 is determined by the requirement that χ does not overclose the universe upon freezeout. However α_2 can in fact be much larger than this minimum value because late decays of η can replenish an initially depleted population of χ particles.

In Fig. 4 we show the constraints in the m_χ–α_2 plane for the case $m_\eta > 3m_\chi$ and $\mu = 0$ (so that semi-annihilation $\chi\chi \to \chi^* h$ is absent). Along the thick solid line the relic abundance of χ is in concordance with that inferred from observation, $\Omega_{\chi+\chi^*} = \Omega_{DM}^{\mathrm{WMAP}}$. The region below is excluded since $\Omega_{\chi+\chi^*} > \Omega_{DM}^{\mathrm{WMAP}}$. In the region above, the decay $\eta \to 3\chi^{(*)}$ must source the relic abundance to obtain $\Omega_{\chi+\chi^*} = \Omega_{DM}^{\mathrm{WMAP}}$ and thus a viable cosmology. We see that, except near the resonance, $2m_\chi \simeq m_h = 120$ GeV, the Higgs portal coupling α_2 must be sizable. The shaded region is excluded due to measurements of past direct detection experiments. In particular, the light DM region with $m_\chi \lesssim 10$ GeV is most constrained by XENON10 (as well as by the CDMS-II low threshold analysis [38]), while heavier DM is most constrained by the XENON100 first run with 11 live days (as well as the final exposure of CDMS-II [37]). We also show the projections for the upcoming release of XENON100 one-year data, as well as a future ton-scale xenon experiment. While the former is not expected to improve upon the XENON10 low-mass limit, the latter will not only improve upon this limit but will essentially probe all values of m_χ that lie to the right of the Higgs resonance region. Finally, the dotted horizontal line shows the requirement that the electroweak vacuum (7) is a global minimum; values of α_2 above that line will make the vacuum configuration metastable. The bound depends on the quartic coupling λ_3 (here $\lambda_3 = 2$) and also on the sign of α_2.

3.3. Constraints for $m_\eta < 3m_\chi$

If $m_\eta < 3m_\chi$, there are two DM species since the decay $\eta \to 3\chi^{(*)}$ is kinematically forbidden. The individual relic abundances of η and $\chi^{(*)}$ are not constrained by WMAP, and so it may appear that further model assumptions are necessary to constrain the two-component scenario. In fact, robust direct detection constraints exist for the lightest DM species independent of the fractional composition of the cosmological dark matter. For the sake of discussion, let us assume that η is the lightest DM particle, $m_\eta < m_\chi$. As discussed in detail above, the only kinematically favorable annihilation channel for η is into the light SM states (11). This means that η must have a minimum Higgs portal coupling α_1. Because the same coupling α_1 controls the DM-nucleon scattering cross section (20), direct detection experiments constrain large portions of the m_η–α_1 parameter space.

In Fig. 5 we show constraints in the m_η–α_1 plane for the case $m_\eta < m_\chi$. The lines as labeled are analogous to the ones shown in the previous Fig. 4. This time, however, the regions between 6 GeV $\lesssim m_\eta \lesssim$ 50 GeV and 70 GeV $\lesssim m_\eta \lesssim$ 80 GeV are excluded for *all* values of α_1. This may seem counterintuitive at first sight, since as α_1 increases the relic abundance decreases: $\Omega_\eta \sim 1/\langle\sigma v\rangle_{\eta\eta\to X_{SM}} \propto \alpha_1^{-2}$ so that $\rho_\eta \propto \alpha_1^{-2}$ by Eq. (21). This can also be seen by the contour lines parallel to the thick solid line which now show decreasing fractions 0.1 and 0.01 (from bottom to top) of the DM abundance. For increasing α_1 there is, however, a corresponding increase in the DM-nucleon scattering cross section (20): $\sigma_n^\eta \propto \alpha_1^2$. Since $dR_\eta/dE_R \propto \rho_\eta \sigma_n^\eta$ the dependence on α_1 cancels out in the nuclear scattering rate (18). This explains why the various direct detection constraints as labeled are now near-to-vertical lines.

While the constraints on the lightest DM particle (assumed to be η for the discussion) are not strongly dependent on the assumptions made about other model parameters, the same is not true for the heavier species (here assumed to be χ). This is because the coupling α_2 governing the interactions of χ with the SM is largely unconstrained by the cosmology, since χ may efficiently deplete through DM conversion processes (*e.g.*, $\chi\chi \to \chi^*\eta$, etc.). Hence further assumptions must be made about other couplings in the Lagrangian (6) to make concrete statements about the heavier DM component.

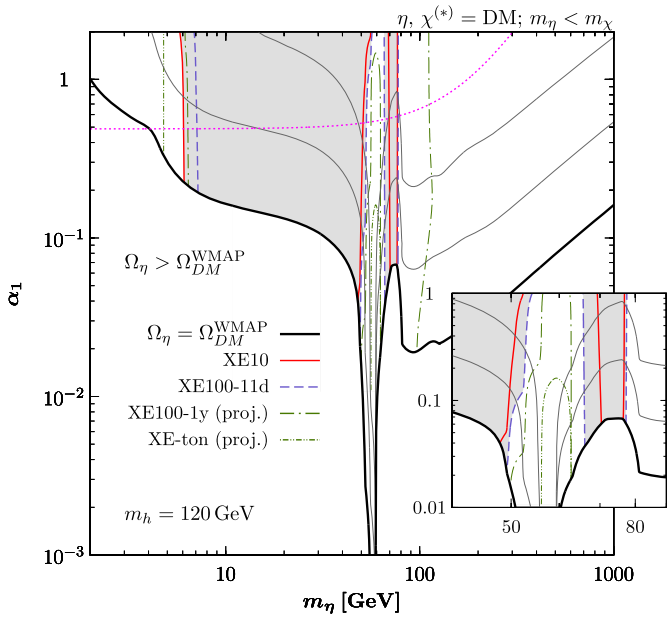

Fig. 5. *Direct detection constraints*: Shown is the m_η–α_1 plane for $m_\eta < m_\chi$. Along (below) the thick solid line $\Omega_\eta = \Omega_{DM}^{\rm WMAP}$ ($\Omega_\eta > \Omega_{DM}^{\rm WMAP}$) holds. The thin gray lines parallel and above are contours with a fraction of 0.1 and 0.01 of $\Omega_{DM}^{\rm WMAP}$ (bottom to top.) The near-to-vertical lines depict the individual experiments and show their current (projected) sensitivity for exclusion. The Higgs resonance region is shown more closely in the inlay.

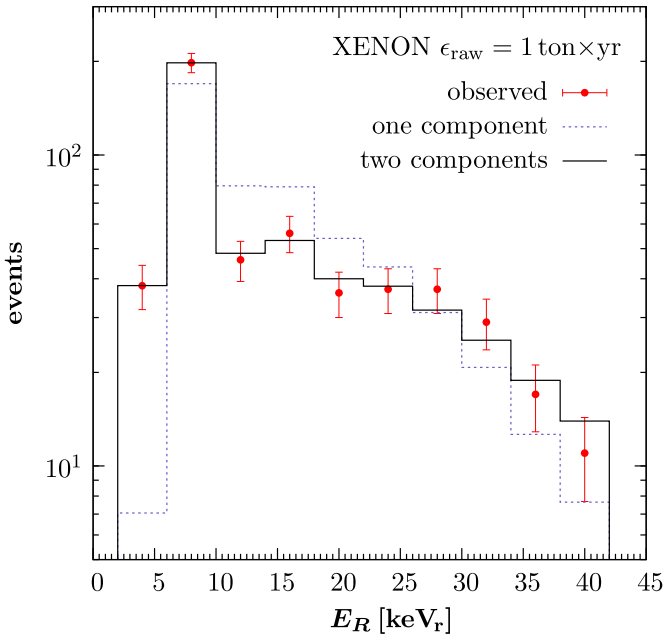

Fig. 6. *Recoil spectrum*: The dots show a Monte Carlo generated recoil spectrum of the two-component DM scenario with input values $m_\eta = 5$ GeV, $\alpha_1 = 0.45$, $m_\chi = 200$ GeV, $\alpha_2 = 0.065$, and $\rho_{1,2} = \rho_0/2$ for a ton-scale liquid Xe detector with raw exposure of 1 ton × yr. The dashed line (blue) shows the attempt to explain the data with a generic single DM particle. The solid line (black) is obtained from a DM model with two components; see main text for details. (For interpretation of the references to color in this figure legend, the reader is referred to the web version of this Letter.)

3.4. Discovering two-component dark matter

The two-component nature of DM for $m_\eta < 3m_\chi$ is one of the most intriguing features of the non-Abelian D_3 discrete symmetry. Naturally, the question arises: can one discriminate between a single-component and a two-component DM scenario at future direct detection experiments? Here we will attempt to provide a quantitative answer to this question. Our analysis will be based on the shape of the nuclear recoil spectrum, which may exhibit distinct features depending on whether one or two components are scattering in the detector.

To answer the question posed above we Monte Carlo generate a sample recoil spectrum for a ton-scale liquid xenon experiment with $m_\eta = 5$ GeV and $m_\chi = 200$ GeV. We further set $\alpha_1 = 0.45$, $\alpha_2 = 0.065$ and $\alpha_4 = 0.3$ for which the dark matter is distributed equally, $\Omega_\eta = \Omega_\chi = \Omega_{DM}^{\rm WMAP}/2$ (note that DM conversion is used to deplete χ). This parameter point is consistent with current direct detection constraints (see Fig. 5). Since the XENON experiments have a poor energy resolution, the bin-width is chosen to be 4 keV$_r$ with a total number of ten bins, starting from 2 keV$_r$. The total number of events to be generated is then drawn from a Poisson distribution with its mean given by the number of theoretically expected events. A sample "experimental" spectrum is shown by the dots in Fig. 6. The events in the first bin are dominated by scatterings of the light state η on the Xe target. In the second bin both states η and $\chi^{(*)}$ contribute equally. At higher recoil energies all events are essentially due to $\chi^{(*)}$. This behavior can of course be traced back to the favorable relation $m_\eta \ll m_\chi$ which yields rather distinct exponential forms of dR/dE_R.

We now attempt to discriminate the two-component origin of the generated spectrum from a single-component DM hypothesis. For this we minimize the Poisson log-likelihood function

$$\chi^2_\lambda = 2 \sum_{\text{bins } i} \left[N_i^{\rm th} - N_i^{\rm obs} + N_i^{\rm obs} \ln\left(N_i^{\rm obs}/N_i^{\rm th}\right)\right] \tag{22}$$

to obtain the best fit and also to assess the goodness-of-the-fit [43]. Here, $N_i^{\rm obs}$ ($N_i^{\rm th}$) is the number of observed (theoretically predicted) events in the i-th bin. We use the program MINUIT [44] to minimize (22). Note that with the procedure outlined above, we only account for statistical uncertainties in the event rate; a more detailed analysis incorporating systematic uncertainties goes well beyond the present scope.

We first attempt to fit the generated recoil spectrum with a single DM particle. The DM mass and spin independent DM-nucleon cross section are used as the fitting parameters. Using the procedure described above, one obtains the dotted (blue) histogram in Fig. 6. As can already be seen by eye, the one-component fit is poor. Indeed, from the goodness-of-fit test the single-DM hypothesis is rejected with confidence well above 99%.

We now turn to a two-component DM model. In this case the recoil spectrum depends on the DM masses m_i, cross sections, $\sigma_n^{(i)}$, and local densities ρ_i, with $i = 1, 2$ and subject to the constraint $\rho_1 + \rho_2 = \rho_0$. Thus, there are in principle five parameters to be inferred from the data of Fig. 6. There exist, however, degeneracies between different parameters in the two-component spectrum so that only certain combinations are accessible. To understand this it is helpful to examine the parametric dependence of the recoil spectrum (18) on m_i, ρ_i, and $\sigma_n^{(i)}$. Using (20), and in the limit of $|\boldsymbol{v}_e| = 0$ and $v_{\rm esc} \to \infty$ one finds

$$\frac{dR_i}{dE_R} \propto \frac{\rho_i \sigma_n^{(i)}}{m_i} \exp\left[-\left(1 + \frac{m_N}{m_i}\right)^2 \frac{E_R}{2 m_N v_0^2} \right], \tag{23}$$

where v_0 is the DM velocity dispersion. Observe that 1) only the product $\rho_i \sigma_n^{(i)}$ enters in dR/dE_R and 2) the exponential shape of the spectrum becomes independent of the DM mass for $m_i \gg m_N$. From the first observation it is clear that one cannot independently determine both ρ_i and $\sigma_n^{(i)}$, but only the product. The second

observation suggests that a second degeneracy between $\rho_i \sigma_n^{(i)}$ and m_i develops once $m_i \gtrsim m_N$. Therefore, further assumptions about the model parameters are required if one desires to break these degeneracies. Fixing, for example, mass and density of the heavier DM to its input values, one then easily recovers all remaining model parameters within a "1σ"-range or better. The result of this fit is shown by the solid (black) histogram in Fig. 6.

Note that the successful determination of the parameters of the lighter state required that at least two bins were populated. If one tried to fit the light DM particle to a single bin, many combinations (m_1, σ_1) would reproduce the signal thus leading to a high degree of degeneracy in m_1 and σ_1. In this regard, it is important to note that—complementary to liquid noble gas experiments—potential future ton-scale cryogenic detectors such as superCDMS [45] or EURECA [46] may be very powerful in disentangling the parameters of a multi-component DM scenario. The reason lies in a much better energy resolution. For example, Ref. [42] estimates for a ton-scale Ge detector $\sigma_{\rm Ge} < 0.5$ keV ($E_R \leqslant 40$ keV). This will allow one to obtain a more detailed picture on the spectral shape of the signal. Moreover, a different target mass with respect to Xe may prove most valuable when attempting to draw differential conclusions by combining results from both detector designs.

4. Discussion

In this Letter we have investigated the simplest model in which DM is stabilized by a non-Abelian discrete symmetry. The model is based on the symmetry group D_3, which is the smallest non-Abelian finite group. The non-Abelian nature of this theory manifests itself in the matter content and interactions of the dark sector, which leads to multi-component DM and a novel early universe cosmology. Robust constraints from direct detection experiments exist for the lightest DM species, and the two-component nature of DM can potentially be tested at future ton-scale experiments.

While we have focused on the phenomenology relevant for direct detection experiments, the D_3 model also has implications for high energy colliders and indirect detection probes. At colliders, the most important consequence of the D_3 model, like other models in which DM couples to the SM through the Higgs portal, is to cause the Higgs boson to decay invisibly if kinematically allowed. An invisibly decaying Higgs boson can be discovered using the vector boson fusion and ZH production channels at the LHC ($\sqrt{s} = 14$ TeV) with 30 fb^{-1} of data [47]. Another generic DM collider probe is a monojet produced in association with pairs of dark matter particles [48,49]. In scalar singlet DM models, this occurs via gluon fusion accompanied by emission of a jet. While the Tevatron is not sensitive to the monojet signature in this class of DM models, the LHC could potentially probe regions with large Higgs portal couplings $\alpha_{1,2} \sim O(1)$ [49]. We also note that a more complete study of the monojet signature in Higgs portal DM models going beyond the effective field theory approach is warranted given that a relatively light Higgs and a top quark loop enter into the amplitude.

A potential indirect probe of the D_3 model is to observe gamma rays from annihilating η or χ particles. In particular, Fermi-LAT data on the isotropic gamma-ray diffuse emission [50], depending on various astrophysical assumptions, can constrain low mass < 10 GeV DM particles annihilating through the Higgs portal [51]. For such constraints to be relevant, the lightest component should carry most of the cosmic DM abundance, since the gamma-ray flux scales as the square of the DM density. In particular, light DM particles with very large Higgs portal couplings will be depleted efficiently and therefore not subject to such constraints. Another possibility is to observe monochromatic gamma-ray lines via $\eta\eta, \chi\chi^* \to h^* \to \gamma\gamma$. This has been studied in Ref. [52], and Fermi-LAT data allows one to probe the model deep within the resonance region $m_{\eta,\chi} \sim m_h/2$.

There are many directions for future investigations with DM and non-Abelian discrete symmetries. Within the minimal D_3 model it would be interesting to consider the case in which η (χ) condense, leading to the spontaneous breaking of the D_3 symmetry to the Z_3 (Z_2) subgroup. This will still lead to a viable model of DM and likely will have distinct signatures compared to the unbroken D_3 symmetry. It would also be interesting to explore larger non-Abelian finite groups, and ultimately non-Abelian discrete gauge symmetries as the origin of DM stability. Finally, given that non-Abelian discrete symmetries may underlie the patterns observed in the quark and lepton masses and mixings, it is interesting to speculate that DM stability may intimately be connected to flavor symmetries.

Stability on cosmological time scales constitutes one of the few and robust guiding principles in formulation of a theory of dark matter. Alternatives to the canonical Z_2-parity symmetry may lead to new phenomena associated with dark matter, as has been clearly demonstrated by our study of the minimal model of D_3 dark matter. We anticipate that new data from a variety of experimental and observational fronts will soon bring us closer in unraveling the particle nature of dark matter and the symmetry which protects its lifetime.

Acknowledgements

We thank Francesco D'Eramo, Andreas Hohenegger, Chris Jillings, Alexander Kartavtsev, Rafael Lang, Maxim Pospelov, and Jesse Thaler for helpful discussions and correspondence. Research at the Perimeter Institute is supported in part by the Government of Canada through NSERC and by the Province of Ontario through MEDT. Research at Max-Planck-Institut für Kernphysik is supported by DFG-Sonderforschungsbereich Transregio 27.

Appendix A. Boltzmann equations

The Boltzmann equation describing the evolution of the number density n_i is given by

$$\frac{dn_i}{dt} + 3Hn_i = C_i, \tag{A.1}$$

where $i = \eta, \chi$ and $H(T)$ is the Hubble parameter accounting for dilution of n_i due to the cosmological expansion of the universe. The collision terms C_i have the following contributions:

$$C_\eta = C_{\eta\eta\to X_{SM}} + C_{\eta\eta\to\chi\chi^*} + C_{\eta\chi\to\chi^*\chi^*} + C_{\eta\chi^*\to\chi\chi} + C_{\eta\to\chi\chi\chi} + C_{\eta\to\chi^*\chi^*\chi^*}, \tag{A.2}$$

$$C_\chi = C_{\chi\chi^*\to X_{SM}} + C_{\chi\chi\to h\chi^*} + C_{\chi h\to\chi^*\chi^*} + C_{\chi\chi^*\to\eta\eta} + C_{\chi\eta\to\chi^*\chi^*} + C_{\chi\chi\to\eta\chi^*} + C_{\chi\chi\chi\to\eta}. \tag{A.3}$$

If the reheating temperature of the radiation dominated universe was high enough, all particles in consideration were once in thermal equilibrium. Assuming Maxwell–Boltzmann statistics and instant thermalization of the reaction products, C_i can be written in familiar, integrated form. Furthermore, CP invariance relates various collision terms so that we find for the individual contributions of C_η:

$$C_{\eta\eta\to X_{SM}} = -\langle\sigma v\rangle_{\eta\eta\to X_{SM}}\left[n_\eta^2 - \left(n_\eta^{\rm eq}\right)^2\right],$$

$$C_{\eta\eta\to\chi\chi^*} = -\langle\sigma v\rangle_{\eta\eta\to\chi\chi^*}\left[n_\eta^2 - \frac{n_\chi^2}{\left(n_\chi^{\rm eq}\right)^2}\left(n_\eta^{\rm eq}\right)^2\right],$$

$$C_{\eta\chi\to\chi^*\chi^*} = -\langle\sigma v\rangle_{\eta\chi\to\chi^*\chi^*}\left[n_\eta n_\chi - \frac{n_\chi^2}{n_\chi^{\rm eq}} n_\eta^{\rm eq}\right],$$
$$C_{\eta\chi^*\to\chi\chi} = C_{\eta\chi\to\chi^*\chi^*},$$
$$C_{\eta\to\chi\chi\chi} = -\langle\Gamma_{\eta\to 3\chi}\rangle\left[n_\eta - \frac{n_\chi^3}{\left(n_\chi^{\rm eq}\right)^3} n_\eta^{\rm eq}\right],$$
$$C_{\eta\to\chi^*\chi^*\chi^*} = C_{\eta\to\chi\chi\chi}, \tag{A.4}$$

while the terms in C_χ in Eq. (A.3) are written as

$$C_{\chi\chi^*\to X_{SM}} = -\langle\sigma v\rangle_{\chi\chi^*\to X_{SM}}\left[n_\chi^2 - \left(n_\chi^{\rm eq}\right)^2\right],$$
$$C_{\chi\chi\to h\chi^*} = -\langle\sigma v\rangle_{\chi\chi\to h\chi^*}\left[n_\chi^2 - n_\chi n_\chi^{\rm eq}\right],$$
$$C_{\chi h\to\chi^*\chi^*} = -\frac{1}{2} C_{\chi\chi\to h\chi^*},$$
$$C_{\chi\chi^*\to\eta\eta} = -\langle\sigma v\rangle_{\chi\chi^*\to\eta\eta}\left[n_\chi^2 - \frac{n_\eta^2}{\left(n_\eta^{\rm eq}\right)^2}\left(n_\chi^{\rm eq}\right)^2\right],$$
$$C_{\chi\chi\to\eta\chi^*} = -\langle\sigma v\rangle_{\chi\chi\to\eta\chi^*}\left[n_\chi^2 - \frac{n_\eta}{n_\eta^{\rm eq}} n_\chi n_\chi^{\rm eq}\right],$$
$$C_{\chi\eta\to\chi^*\chi^*} = -\frac{1}{2} C_{\chi\chi\to\eta\chi^*},$$
$$C_{\chi\chi\chi\to\eta} = -3C_{\eta\to 3\chi}. \tag{A.5}$$

The thermally averaged annihilation cross section for process $a+b\to c+d$ is in general given by

$$\langle\sigma v\rangle_{ab} = \frac{1}{8m_a^2 m_b^2 T K_2(m_a/T) K_2(m_b/T)} \times \int_{(m_a+m_b)^2}^{\infty} ds\, W_{ab}\, p_{ab} K_1\left(\frac{\sqrt{s}}{T}\right), \tag{A.6}$$

where the quantity W_{ab} is defined as

$$W_{ab} = \frac{1}{g_a g_b}\left(\frac{1}{8\pi S_{cd}}\frac{\lambda^{1/2}(s,m_c^2,m_d^2)}{s}\right) \times \sum_{spins}\int_{-1}^{1}\frac{d\cos\theta}{2}\left|\mathcal{M}_{ab\to cd}(\cos\theta)\right|^2. \tag{A.7}$$

In W_{ab} the squared matrix element $|\mathcal{M}_{ab\to cd}|^2$ is integrated over the c.m. scattering angle θ. K_i denotes the modified Bessel function of order i and p_{ab} is the momentum of relative motion of a and b. Furthermore, g_a, g_b are the number of internal degrees of freedom, S_{cd} is a symmetry factor accounting for identical final states, and $\lambda(\hat{x},\hat{y},\hat{z}) \equiv \hat{x}^2+\hat{y}^2+\hat{z}^2-2\hat{x}\hat{y}-2\hat{x}\hat{z}-2\hat{y}\hat{z}$. For the decay $a\to b+c+\cdots$, the thermal average reads

$$\langle\Gamma_{a\to b+c+\cdots}\rangle = \frac{K_1(m_a/T)}{K_2(m_a/T)}\Gamma_{a\to b+c+\cdots}, \tag{A.8}$$

where $\Gamma_{a\to b+c+\cdots}$ is the standard decay rate for a particle a at rest.

References

[1] See *e.g.* G. Jungman, M. Kamionkowski, K. Griest, Phys. Rep. 267 (1996) 195, arXiv:hep-ph/9506380;
G. Bertone, D. Hooper, J. Silk, Phys. Rep. 405 (2005) 279, arXiv:hep-ph/0404175.
[2] B. Batell, Phys. Rev. D 83 (2011) 035006, arXiv:1007.0045 [hep-ph].
[3] M. Lisanti, J.G. Wacker, arXiv:0704.2816 [hep-ph].
[4] N. Haba, Y. Kajiyama, S. Matsumoto, H. Okada, K. Yoshioka, Phys. Lett. B 695 (2011) 476, arXiv:1008.4777 [hep-ph].
[5] Y. Kajiyama, H. Okada, arXiv:1011.5753 [hep-ph].
[6] T. Hambye, JHEP 0901 (2009) 028, arXiv:0811.0172 [hep-ph];
T. Hambye, M.H.G. Tytgat, Phys. Lett. B 683 (2010) 39, arXiv:0907.1007 [hep-ph].
[7] F. Chen, J.M. Cline, A.R. Frey, Phys. Rev. D 79 (2009) 063530, arXiv:0901.4327 [hep-ph];
F. Chen, J.M. Cline, A.R. Frey, Phys. Rev. D 80 (2009) 083516, arXiv:0907.4746 [hep-ph].
[8] D.G.E. Walker, arXiv:0907.3146 [hep-ph];
D.G.E. Walker, arXiv:0907.3142 [hep-ph].
[9] M. Hirsch, S. Morisi, E. Peinado, J.W.F. Valle, arXiv:1007.0871 [hep-ph];
D. Meloni, S. Morisi, E. Peinado, arXiv:1011.1371 [hep-ph];
M.S. Boucenna, M. Hirsch, S. Morisi, E. Peinado, M. Taoso, J.W.F. Valle, arXiv:1101.2874 [hep-ph].
[10] T. Schwetz, M.A. Tortola, J.W.F. Valle, New J. Phys. 10 (2008) 113011, arXiv:0808.2016 [hep-ph].
[11] G. Altarelli, F. Feruglio, Rev. Mod. Phys. 82 (2010) 2701, arXiv:1002.0211 [hep-ph].
[12] H. Ishimori, T. Kobayashi, H. Ohki, Y. Shimizu, H. Okada, M. Tanimoto, Prog. Theor. Phys. Suppl. 183 (2010) 1, arXiv:1003.3552 [hep-th].
[13] B.A. Ovrut, J. Math. Phys. 19 (1978) 418;
G. Etesi, J. Math. Phys. 37 (1996) 1596, hep-th/9706029;
M. Koca, M. Al-Barwani, R. Koc, J. Phys. A 30 (1997) 2109;
M. Koca, R. Koc, H. Tutunculer, Int. J. Mod. Phys. A 18 (2003) 4817, hep-ph/0410270;
A. Adulpravitchai, A. Blum, M. Lindner, JHEP 0909 (2009) 018, arXiv:0907.2332 [hep-ph];
J. Berger, Y. Grossman, JHEP 1002 (2010) 071, arXiv:0910.4392 [hep-ph];
C. Luhn, arXiv:1101.2417 [hep-ph].
[14] T. Watari, T. Yanagida, Phys. Lett. B 544 (2002) 167, hep-ph/0205090;
T. Watari, T. Yanagida, Phys. Lett. B 532 (2002) 252, hep-ph/0201086;
G. Altarelli, F. Feruglio, Y. Lin, Nucl. Phys. B 775 (2007) 31, hep-ph/0610165;
T. Kobayashi, H.P. Nilles, F. Ploger, S. Raby, M. Ratz, Nucl. Phys. B 768 (2007) 135, hep-ph/0611020;
A. Adulpravitchai, A. Blum, M. Lindner, JHEP 0907 (2009) 053, arXiv:0906.0468 [hep-ph];
T.J. Burrows, S.F. King, Nucl. Phys. B 835 (2010) 174, arXiv:0909.1433 [hep-ph];
A. Adulpravitchai, M.A. Schmidt, JHEP 1101 (2011) 106, arXiv:1001.3172 [hep-ph];
T.J. Burrows, S.F. King, Nucl. Phys. B 842 (2011) 107, arXiv:1007.2310 [hep-ph];
H. Abe, K.-S. Choi, T. Kobayashi, H. Ohki, M. Sakai, arXiv:1009.5284 [hep-th].
[15] V. Silveira, A. Zee, Phys. Lett. B 161 (1985) 136.
[16] J. McDonald, Phys. Rev. D 50 (1994) 3637, arXiv:hep-ph/0702143.
[17] C.P. Burgess, M. Pospelov, T. ter Veldhuis, Nucl. Phys. B 619 (2001) 709, arXiv:hep-ph/0011335.
[18] A. Blum, C. Hagedorn, M. Lindner, Phys. Rev. D 77 (2008) 076004, arXiv:0709.3450 [hep-ph].
[19] P.H. Frampton, T.W. Kephart, Int. J. Mod. Phys. A 10 (1995) 4689, arXiv:hep-ph/9409330.
[20] M. Gonderinger, Y. Li, H. Patel, M.J. Ramsey-Musolf, JHEP 1001 (2010) 053, arXiv:0910.3167 [hep-ph].
[21] C.E. Yaguna, Phys. Rev. D 81 (2010) 075024, arXiv:1003.2730 [hep-ph].
[22] F. D'Eramo, J. Thaler, JHEP 1006 (2010) 109, arXiv:1003.5912 [hep-ph].
[23] M. Fairbairn, J. Zupan, JCAP 0907 (2009) 001, arXiv:0810.4147 [hep-ph].
[24] P. Gondolo, G. Gelmini, Nucl. Phys. B 360 (1991) 145.
[25] J. Edsjo, P. Gondolo, Phys. Rev. D 56 (1997) 1879, arXiv:hep-ph/9704361.
[26] P. Gondolo, J. Edsjo, P. Ullio, L. Bergstrom, M. Schelke, E.A. Baltz, JCAP 0407 (2004) 008, arXiv:astro-ph/0406204.
[27] M.A. Luty, Phys. Rev. D 45 (1992) 455.
[28] E. Komatsu, et al., arXiv:1001.4538 [astro-ph.CO].
[29] M. Pospelov, J. Pradler, Annu. Rev. Nucl. Part. Sci. 60 (2010) 539, arXiv:1011.1054 [hep-ph].
[30] M. Kawasaki, K. Kohri, T. Moroi, Phys. Rev. D 71 (2005) 083502, astro-ph/0408426;
K. Jedamzik, Phys. Rev. D 74 (2006) 103509, hep-ph/0604251;
F.D. Steffen, JCAP 0609 (2006) 001, hep-ph/0605306;
R.H. Cyburt, J. Ellis, B.D. Fields, F. Luo, K.A. Olive, V.C. Spanos, JCAP 0910 (2009) 021, arXiv:0907.5003 [astro-ph.CO];
M. Pospelov, J. Pradler, arXiv:1010.4079 [astro-ph.CO].
[31] J.D. Lewin, P.F. Smith, Astropart. Phys. 6 (1996) 87.
[32] J.R. Ellis, K.A. Olive, C. Savage, Phys. Rev. D 77 (2008) 065026, arXiv:0801.3656 [hep-ph].
[33] S. Profumo, K. Sigurdson, L. Ubaldi, JCAP 0912 (2009) 016, arXiv:0907.4374 [hep-ph].
[34] J. Angle, et al., XENON Collaboration, Phys. Rev. Lett. 100 (2008) 021303, arXiv:0706.0039 [astro-ph].
[35] J. Angle, et al., XENON10 Collaboration, Phys. Rev. D 80 (2009) 115005, arXiv:0910.3698 [astro-ph.CO].
[36] E. Aprile, et al., XENON100 Collaboration, Phys. Rev. Lett. 105 (2010) 131302, arXiv:1005.0380 [astro-ph.CO].

[37] Z. Ahmed, et al., CDMS-II Collaboration, Science 327 (2010) 1619, arXiv:0912.3592 [astro-ph.CO].
[38] Z. Ahmed, et al., CDMS-II Collaboration, arXiv:1011.2482 [astro-ph.CO].
[39] J.I. Collar, arXiv:1010.5187 [astro-ph.IM];
C. Savage, arXiv:1012.3926 [astro-ph.CO].
[40] P. Sorensen, JCAP 1009 (2010) 033, arXiv:1007.3549 [astro-ph.IM].
[41] S. Yellin, Phys. Rev. D 66 (2002) 032005, physics/0203002.
[42] M. Pato, L. Baudis, G. Bertone, R.R. de Austri, L.E. Strigari, R. Trotta, arXiv:1012.3458 [astro-ph.CO].
[43] S. Baker, R.D. Cousins, Nuclear Instrum. Methods Phys. Res. 221 (2) (1984) 437.
[44] F. James, M. Roos, Comput. Phys. Commun. 10 (1975) 343.
[45] T. Bruch, for the CDMS Collaboration, arXiv:1001.3037 [astro-ph.IM].
[46] http://www.eureca.ox.ac.uk.
[47] G. Aad, et al., ATLAS Collaboration, arXiv:0901.0512 [hep-ex].
[48] M. Beltran, D. Hooper, E.W. Kolb, Z.A.C. Krusberg, T.M.P. Tait, JHEP 1009 (2010) 037, arXiv:1002.4137 [hep-ph];
J. Goodman, M. Ibe, A. Rajaraman, W. Shepherd, T.M.P. Tait, H.B.P. Yu, Phys. Lett. B 695 (2011) 185, arXiv:1005.1286 [hep-ph];
Y. Bai, P.J. Fox, R. Harnik, JHEP 1012 (2010) 048, arXiv:1005.3797 [hep-ph].
[49] J. Goodman, M. Ibe, A. Rajaraman, W. Shepherd, T.M.P. Tait, H.B.P. Yu, Phys. Rev. D 82 (2010) 116010, arXiv:1008.1783 [hep-ph].
[50] A.A. Abdo, et al., Fermi-LAT Collaboration, JCAP 1004 (2010) 014, arXiv:1002.4415 [astro-ph.CO].
[51] C. Arina, M.H.G. Tytgat, JCAP 1101 (2011) 011, arXiv:1007.2765 [astro-ph.CO];
K.N. Abazajian, S. Blanchet, J.P. Harding, arXiv:1011.5090 [hep-ph].
[52] S. Profumo, L. Ubaldi, C. Wainwright, Phys. Rev. D 82 (2010) 123514, arXiv:1009.5377 [hep-ph].